Available online at www.sciencedirect.com
ScienceDirect
Journal of Catalysis 253 (2008) 261–268
JOURNAL OF CATALYSIS
www.elsevier.com/locate/jcat

Kinetic and spectroscopic study of methane combustion over α-Mn_2O_3 nanocrystal catalysts

Yi-Fan Han *, Luwei Chen, Kanaparthi Ramesh, Effendi Widjaja, Srilakshmi Chilukoti, Ingrid Kesumawinata Surjami, Junsong Chen

Institute of Chemical and Engineering Sciences, 1, Pesek Road, Jurong Island, 627833 Singapore

Received 12 November 2007; accepted 13 November 2007

Abstract

The kinetics of methane combustion was investigated on bulk and α-Mn_2O_3 nanocrystal catalysts using a fixed bed microreactor. The kinetic behavior is profoundly affected by changes in the particle size of α-Mn_2O_3 from 0.5 μm to ca. 50 nm. Real-time in situ Raman spectroscopy was used to probe the structure of both catalysts during the reaction. A reversible phase-transformation from α-Mn_2O_3 to a Mn_3O_4-like species, as evidenced by the presence of a band at 648 cm^{-1} in He flow and at 660 cm^{-1} in methane combustion, was observed for α-Mn_2O_3 nanocrystals only at or above 450 °C. This modification is probably due to the loss of lattice oxygen at high temperatures, leading to structural reconstruction. We infer from the study that the phase change of the α-Mn_2O_3 nanocrystal catalyst might be responsible for the decrease of E_a and the near zero-order dependence on oxygen partial pressure, and might be associated with the activation of the C–H bonds in methane.

Keywords: Kinetics; Raman spectroscopy; In situ; Reverse phase-transfer; Methane combustion; α-Mn_2O_3 nanocrystals

1. Introduction

Natural gas fueled vehicles and turbines are attractive over those that use fossil fuels because they produce lower amount of pollutants such as NO, CO_x and other toxic gases [1–3]. However, complete combustion is necessary since unburned hydrocarbons such as methane (CH_4) can potentially contribute to the global greenhouse effect [3]. Catalytic combustion of CH_4 is a very important reaction in this context, due to its potential for treating the exhaust gases (<0.5% CH_4). Stricter laws are now being enforced to control CH_4 emissions.

Manganese oxide (MnO_x) and its mixture with other oxides (MnO_x–M_xO_y: M = V, Cr, Co, Fe, Cu, Zr) [1,4–13] have been widely used for this reaction. More recently, we have reported that α-Mn_2O_3 nanocrystals (diameter (d): 30–50 nm) showed higher activity than its bulk counterpart (d: ∼0.5 μm) for CH_4 combustion [14], partly, because nanocrystals have high surface to volume ratio. It has also been demonstrated that Mn_2O_3 crystallites with a single phase exhibit remarkable catalytic activity towards other reactions, such as the oxidation of ethylene [15] and carbon monoxide [16,17], and the decomposition of NO_x [18]. Currently, mechanistic understanding of the methane combustion over the α-Mn_2O_3 catalyst is still very limited. Kinetic studies together with in situ spectroscopic analysis are an effective combination for this purpose.

CH_4 is the most stable hydrocarbon towards oxidation among combustible hydrocarbons [19]. The mechanism for CH_4 combustion on MnO_x-based catalysts, especially, the reaction behavior dependence on the structural changes of the catalysts induced by reactants, temperature, and other factors under the reaction conditions, is not clearly understood yet.

Determining the structural changes in MnO_x oxides under reaction conditions is still a challenge because of facile phase-transformations that own at elevated temperatures (>400 °C). Real-time in situ spectroscopic methods suitable for the determination of structure at working temperatures are very attractive. Among these methods, Raman scattering is a particularly useful spectroscopic tool for characterizing metal oxides [20–26]; it has high sensitivity even to a tiny modifications of the

* Corresponding author. Fax: +65 61366182.
E-mail address: han_yi_fan@ices.a-star.edu.sg (Y.-F. Han).

0021-9517/$ – see front matter
doi:10.1016/j.jcat.2007.11.010

structure and suffers little interference from the gas-phase reactants. Several studies [27–33] including our recent works [34] have been conducted on MnO_x using laser Raman spectroscopy (LRS), indicating that the structure might be modified during catalytic reactions. However, convincible evidence is still not available due to the difficulties of applying in situ methods. Radhakrishnan and Oyama [12,27,30,35] have systemically investigated supported manganese oxides during ozone decomposition and oxidation reactions using in situ Raman spectroscopy. However, studies are rare of unsupported MnO_x nanocrystals during CH_4 combustion or other oxidation reactions.

In this study, a nanostructured α-Mn_2O_3 catalyst with coral-like morphology is prepared by oxidative decomposition of $MnCO_3$. The obtained α-Mn_2O_3 nanocrystals are used for kinetic studies and structural characterization. Reaction orders with respect to CH_4 and O_2 are obtained and the apparent activation energies (E_a) are measured in a temperature range of 350–550 °C. Temperature-dependent in situ Raman spectra are recorded during the reaction. The reaction behavior is correlated with the structural modifications of the working catalyst.

2. Experimental

2.1. Catalyst preparation and reactivity measurements

Nanostructured α-Mn_2O_3 was prepared by the direct thermal decomposition of $MnCO_3$ powders (Aldrich, batch no. 13520DD) in static air. Controlled calcination of the $MnCO_3$ powders was carried out at 700 °C for 5 h with a ramping rate of 1 °C/min.

Kinetic measurements were carried out in a micro-plug-flow reactor in a stream of CH_4, O_2 and He with space velocities from 6000 to 36,000 h^{-1} at atmospheric pressure. Prior to each experiment, the catalysts were pretreated in 20 ml/min of Ar flow at 100 °C for 2 h. In order to obtain differential reaction rates, the conversion of CH_4 was controlled below 10% by diluting the catalyst with α-Al_2O_3 powders in ratios ranging from 1 to 9. Absolute mass-specific reaction rates and turnover rates were calculated from the average concentrations of each component $\dot{c}_i$, at the inlet and outlet of the reactor:

$$r_{CH_4} = \frac{\dot{c}_{CH_4,in} \cdot X_{CH_4} \cdot \dot{V}_{gas}}{m_{Mn_2O_3}} \left[\text{mmol}\,h^{-1}\,g_{cat}^{-1}\right], \quad (1)$$

where $m_{Mn_2O_3}$: mass of Mn_2O_3 in the reactor bed, $\dot{V}$: total molar flow rate, X_{CH_4}: conversion of CH_4 based on CO_2 formation, $\dot{c}_{CH_4}$: concentration of CH_4 in gas mixture, equal to p_i/p_0, p_i: partial pressure of reactants, p_0: total pressure in the system.

The turnover rates (s^{-1}) under steady state were calculated using a total active sites of 150 μmol/g for the nanocrystal α-Mn_2O_3 and 67 μmol/g for the bulk one (Aldrich, 99.999%, 4.8 m^2/g of surface area, 0.5 μm of particle size), obtained from the oxygen-desorption experiments.

Analysis of the reactants and products was performed with an online gas chromatograph (Shimadzu GC-2010) equipped with a CP-carbonBOND column. Each data point was taken at an interval of 2 h under steady state reaction conditions. For comparison, the reaction rate over a bulk α-Mn_2O_3 sample was obtained under the same conditions. It is important to note that deactivation was very low for both catalysts. At 550 °C, activity losses of about 5.0% and 2.0% for the bulk and the nanocrystal α-Mn_2O_3 were detected after running for 24 h in a stream of 0.5 kPa CH_4, 3.0 kPa O_2, and He as balance. Since the nanocrystal Mn_2O_3 sample is a very fine powder, only internal diffusion can be considered. According to the Weisz–Prater Criterion [36], where D_{eff} is the effective diffusivity in the Knudsen regime for average pore radii of less than 100 nm, the diffusion coefficient, D_{eff}, for CH_4 at 500 °C over the catalyst is calculated as 3.32×10^{-6} m^2/s by reference to the value measured in a CH_4/He mixture by Hayes et al. [37]. The reaction order in CH_4 is assumed to be unity. The value of $\eta_i\phi^2$ is ca. 0.0639 at 500 °C (0.5 kPa CH_4, 3.0 kPa O_2, rest He), which is lower than 0.15. This indicates that under our experimental conditions the reaction is in the kinetic regime and mass-transfer limitations can be rule out based on the Weisz–Prater Criterion.

2.2. Characterization

2.2.1. LRS

Raman spectra were measured with an in situ setup using a Raman microscope (InVia Reflex, Renishaw) equipped with a thermoelectrically cooled CCD array detector and a high grade Leica microscope (long working distance objective 50×). The sample was placed into a sample cell, specially designed for catalytic reactions at high temperature and pressure (CCR1000, Linkam fitted with quartz windows). The sample was mounted on an unreactive disposable ceramic fabric filter placed inside a ceramic heating element, which was capable of heating samples from ambient up to 1000 °C. The reaction conditions were the same as those for the micro-fixed bed reactor. The gases (3.0 kPa O_2, 0.5 kPa CH_4, diluted in He, or He only) were introduced into the catalyst stage via a 1/16 inch gas line. The gases passed through the sample and ceramic fabric filter at a flow rate of ca. 50 ml/min. The flow rates of the reactant gases were controlled by mass flow controllers. Raman measurements were performed on a sample spot irradiated by a visible 514.5 nm argon ion laser. The laser power from the source was around 25 mW, which is very close to the power (20 mW) previously used for MnO_x characterization [33]. It should be noted that heating induced by the laser, which usually interferes with the acquiring of the real spectroscopy, was controlled carefully. Thus, the laser power was minimized as much as possible by lowering the power using density filter and optimizing the time for scanning without sacrificing too much on the Raman signals. It is estimated that only about 1–2 mW of the laser power reached the samples during the measurements. So, the in situ Raman signals are noisy, and high precision of the peaks at corresponding wave numbers was not available. The signal for the LRS was attenuated significantly above 500 °C. The scanning time for each Raman spectrum was ca. 360 s with a spectral resolution around 1–1.3 cm^{-1}. The temperature ramping rate is 10 °C/min when the sample was heated from 25 to 500 °C. Note that structural changes induced by the laser were ruled

out by taking time-dependent spectra measured in the He atmosphere.

2.2.2. XRD

X-ray diffraction patterns were obtained with a Bruker D8 diffractometer using CuK_α radiation ($\lambda = 1.540589$ Å). The crystal size of the Mn_2O_3 sample was calculated from the width of the diffraction profiles, using the full-width-at-half-maximum (FWHM) of the crystalline peaks of the ⟨222⟩, ⟨440⟩, and ⟨622⟩ reflection using the Debye–Scherrer formula:

$$D = 0.9\lambda/\Delta\cos(\theta), \tag{2}$$

where D: crystal size, λ: wavelength of X-rays, Δ: FWHM of the diffraction peak, θ: angle corresponding to the peak.

2.2.3. SEM

The measurements were performed with a JEOL JSM-6700F field emission scanning electron microscopy. Approximately 200 particles were selected when the average particle size was estimated based on the obtained images.

2.2.4. N_2 adsorption

The surface area of the catalyst was obtained from the adsorption and desorption N_2 isotherms that were collected on an Autosorb-6 at liquid N_2 temperature. Prior to the measurement, all samples were degassed at 300 °C until a stable vacuum of ca. 5 mTorr was reached.

2.2.5. Oxygen-temperature-programmed desorption (TPD)

The TPD experiments were performed in a micro-fixed-bed reactor (quartz reactor with 20 cm long and 0.4 cm diameter) connected to a GC-QMS (HPR-20, Hiden Analytical Ltd.), with which masses (m/e: 16(O_2), 18(H_2O), 28(N_2), 44(CO_2)) were monitored. Prior to the experiments, the catalysts prepared were first pretreated in an air flow of 50 ml/min for 1 h at 200 °C in order to remove weakly adsorbed oxygen and other contaminates, thus is regarded as "O_2-free surface." Then, the samples were cooled to room temperature in a N_2 flow (50 ml/min). The temperature ramped from 25 to 500 °C at a rate of 20 °C/min in the same N_2 flow. In order to determine the total number of active sites, an "O_2-precovered" catalyst was prepared by purging with O_2 (20 ml/min) at room temperature followed by TPD measurements.

3. Results and discussion

3.1. Kinetics

Fig. 1a shows the pressure-dependent reaction rates on partial pressure of O_2 (p_{O_2}) from 3.0 to 10.0 kPa while keeping partial pressure of CH_4 (p_{CH_4}) at 0.5 kPa. For the α-Mn_2O_3 nanocrystals, the reaction rate increased with an increase in p_{O_2}, yielding an order of 0.34 with respect to O_2 (α) at 400 and 450 °C. However, at 500 °C the order was reduced to nearly zero. On the other hand, by keeping p_{O_2} at 3.0 kPa while varying p_{CH_4} from 0.1 to 1.0 kPa (Fig. 1b), the orders with respect

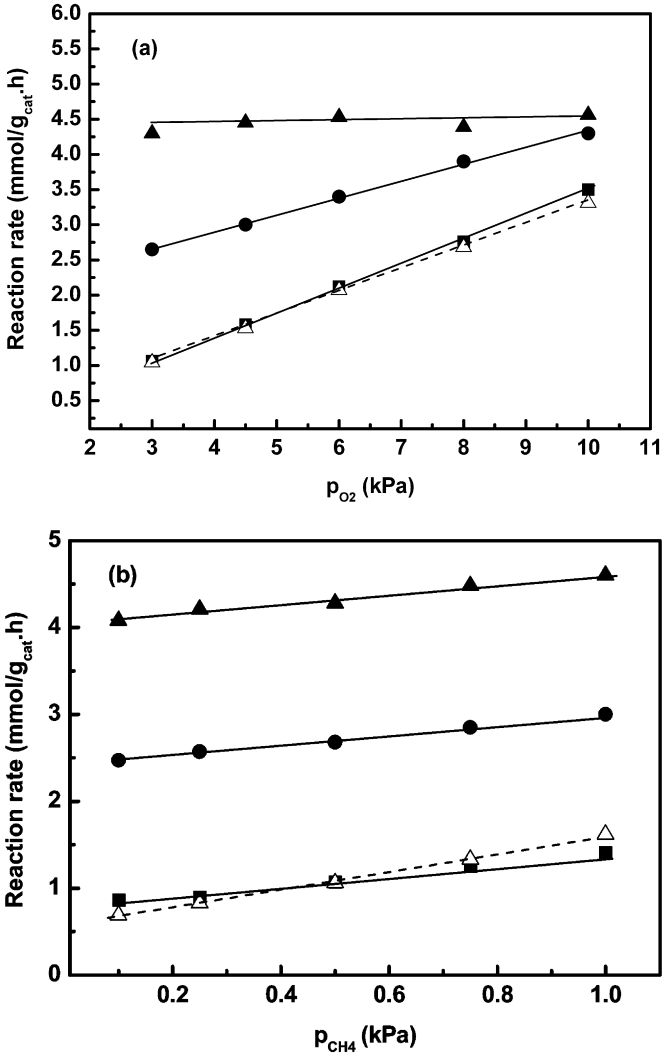

Fig. 1. Dependence of reaction rates (determined via CO_2 formation) on the CH_4 concentration over α-Mn_2O_3 nanocrystals at 400 (■), 450 (●), 500 °C (▲) and over bulk α-Mn_2O_3 at 500 °C (△). (a) 3.0–10.0 kPa O_2, 0.5 kPa CH_4, in He. (b) 0.1–1.0 kPa CH_4, 3.0 kPa O_2, in He. Dilute ratio with α-Al_2O_3 powders: pure to 1/9, GHSV: 6000–36,000 h^{-1}.

to CH_4 (β) were 0.62 at 400 °C and 0.65 at 500 °C. For comparison, reaction orders of 0.32 for O_2 and 0.7 for CH_4 were measured for the bulk α-Mn_2O_3 under the same conditions at 500 °C.

Fig. 2 shows that the rates increased with rise in temperature from 350 to 550 °C over both catalysts. Obviously, the catalytic activity of the α-Mn_2O_3 nanocrystals was much higher than that of the bulk. The Arrhenius plots of CH_4 oxidation rate yield E_a values of 86.5 kJ/mol for the bulk, and 80.7 kJ/mol (350–450 °C) and 47.6 kJ/mol (450–550 °C) for the nanocrystal α-Mn_2O_3.

The performance of the MnO_x catalyst is improved usually through either mixing with rare earth oxides such as LaO_x [35,38–40] or mixing with alkaline earth oxides such as SrO_x [41] and BaO_x [40]. Thus, catalytic properties such as the oxygen storage capacity (OSC) and stability can be significantly improved during the combustion [35,38–40]. How-

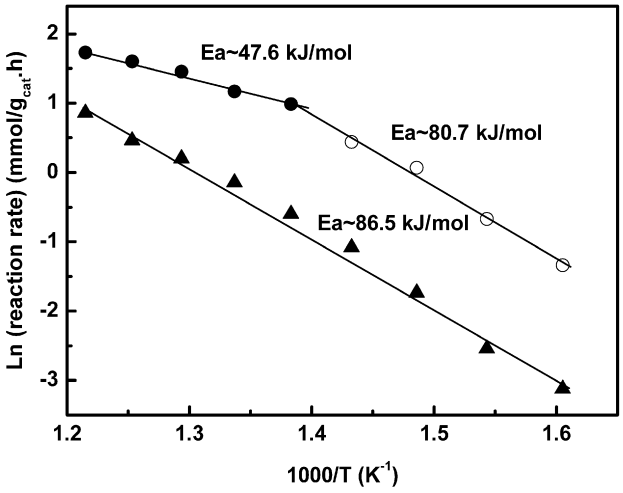

Fig. 2. Arrhenius plots of the reaction rate ($\ln(r)$) vs $1/T$ for CH_4 combustion over bulk α-Mn_2O_3 (▲) and α-Mn_2O_3 nanocrystals (○: 350–450 °C; ●: 450–550 °C). Feed gas: 0.5 kPa CH_4, 3.0 kPa O_2, in He. Dilute ratio with α-Al_2O_3 powders: pure to 1/9, GHSV: 6000–36,000 h^{-1}.

ever, we will not discuss these issues here in order not to divert attention from the focus of this work. The kinetic parameters obtained at similar reaction conditions over several typical MnO_x-based catalysts are listed in Table 1. At 500 °C, common kinetic features are positive reaction orders for both oxygen (0.16–0.32) and methane (0.7–0.9), which are observed for all bulk and supported catalysts. Moreover, except the activation energy measured for a $LaMn_{0.9}O_3$ is 176.1 kJ/mol [41], and the E_a values over all bulk catalysts fall in a narrow range between 82.3 and 102 kJ/mol, indicating that structural modifications of the bulk MnO_x do not change the reaction mechanism. However, a drastic drop of E_a above 450 °C (47.6 kJ/mol) is observed for the first time over the α-Mn_2O_3 nanocrystals. Obviously, the reaction behavior over the MnO_x nanocrystals is different compared to the bulk catalysts. According to the values reported in Table 1, at 500 °C the following order can be derived: $LaMn_{0.9}O_3$ > α-Mn_2O_3 (nanocrystal) > 20% $LaMnO_3$/MgO > $LaMnO_3$ > α-Mn_2O_3 (bulk) ≈ $BaAl_9Mn_3O_{19}$. It is noted that the highest rate for the $LaMn_{0.9}O_3$ catalyst [41] is due to the high partial pressures in the reaction system. Meanwhile, the turnover rate (s^{-1}) over the α-Mn_2O_3 nanocrystals (0.08 s^{-1}) is twice as that for the bulk (0.04 s^{-1}). The kinetic behavior (drastic drop of E_a above 450 °C, near zero-order dependence in O_2 at 500 °C and high rate over the nanocrystal α-Mn_2O_3) and activity for the nanocrystal α-Mn_2O_3 sample are unique in comparison with other bulk and supported MnO_x catalysts for CH_4 combustion. These unique kinetic features for the nanocrystal α-Mn_2O_3 will be discussed further.

3.2. Characterization

Fig. 3 shows that the powder XRD pattern for the nanocrystals is quite stable after the reaction (in 0.5 kPa CH_4, 3.0 kPa O_2, rest He, space velocity of 36,000 h^{-1}, at 550 °C for 10 h). The pattern is identical to that obtained for the bulk, corresponding to the typical bixbyite α-Mn_2O_3 (JCPDS 41-1442). The average particle size was calculated by the Debye–Scherrer formula based on the main reflection peaks for the (222), (440) and (622) planes. The average particle size and surface area of the α-Mn_2O_3 nanocrystals were ca. 50.0 ± 2.0 nm and 19.0 m^2/g, respectively. Moreover, the particle size evaluated from the XRD patterns for all catalysts was comparable with that visualized from SEM (Fig. 4, d: 53.0 ± 3.0 nm).

Ex situ LRS spectra obtained from the fresh and spent catalysts under ambient conditions are shown in Fig. 5. In comparison with the Raman spectroscopy obtained from the bulk [15,16], the bands at 307, 341, 637 and 686 cm^{-1} detected for the nanocrystals may correspond to the out-of-plane bending modes of Mn_2O_3, asymmetric stretching of bridged oxygen species (Mn–O–Mn), and symmetric stretching of Mn_2O_3 groups. Actually, it is very difficult to ascribe any structural modifications from these bands.

Interestingly, the in situ LRS spectra in Fig. 6 showed quite different profiles, which revealed structural modifications during CH_4 combustion. It is noted that useful information can still

Table 1
Comparisons of kinetic parameters for the methane combustion over Mn-based catalysts, power low functionality[a]: $\gamma_{CH_4} = k(p_{O_2}/p_{total})^{\alpha}(p_{CH_4}/p_{total})^{\beta}$

Catalysts	p_{O_2} (kPa)	p_{CH_4} (kPa)	E_a[a] (kJ/mol)	Rate (γ_{CH_4}, TOF)		α	β	Ref.
				(mmol/g h)	(s^{-1})			
$LaMnO_3$	10.0	0.4	102.0	1.18	N.A.[b]	0.16	0.86	[35]
20% $LaMnO_3$/MgO	10.0	0.4	97.4	2.32	N.A.	0.17	0.69	[35]
$La_{0.8}Sr_{0.2}MnO_3$	23.0	2.0	82.3	N.A.	N.A.	0.3	0.9	[38]
$BaAl_9Mn_3O_{19}$	4.0	1.0	87.5	1.03	N.A.	0.3	0.75	[30]
$LaMn_{0.9}O_3$	50	8.3	176.1	7.8	N.A.	N.A.	N.A.	[41]
Mn_2O_3 (bulk)	3.0	0.5	86.5 ± 2.0	1.06	0.04	0.32	0.70	This study
Mn_2O_3 (nano)	3.0	0.5	80.7 ± 2.0[c]	4.28	0.08	0.34	0.62[d]	This study
Mn_2O_3 (nano)	3.0	0.5	47.6 ± 1.8[e]			~0	0.65	This study

[a] E_a was measured in a temperature range of 350–550 °C; reaction rates (partial pressure of reactants was given in column 2) and reaction orders were measured at 500 °C under atmospheric pressure; the turnover rates were calculated using total active sites of 150 μmol/g for the nanocrystal α-Mn_2O_3 and 67 μmol/g for the bulk one.
[b] N.A.: not available.
[c] Temperature range from 350 to 450 °C.
[d] Reaction order at 400 °C.
[e] Temperature range from 450 to 550 °C.

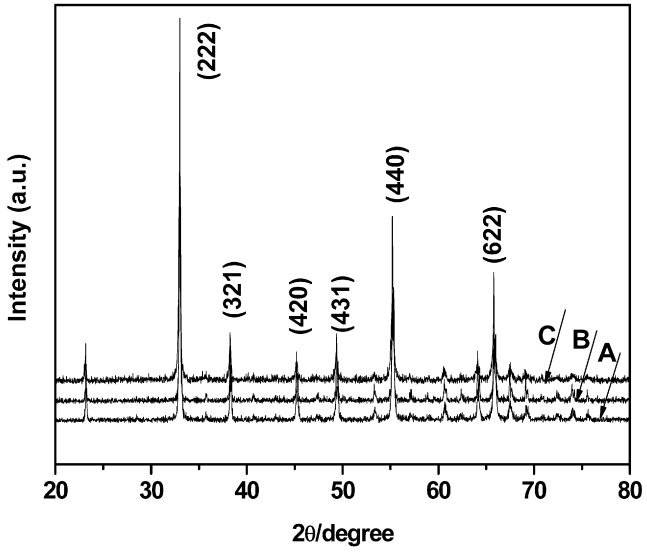

Fig. 3. XRD patterns for the α-Mn_2O_3 nanocrystals (A: fresh, B: spent), and bulk α-Mn_2O_3 (C: fresh). The reaction was carried out in the stream of 0.5 kPa CH_4, 3.0 kPa O_2, in He, space velocity: 36,000 h^{-1}, at 550 °C for 10 h.

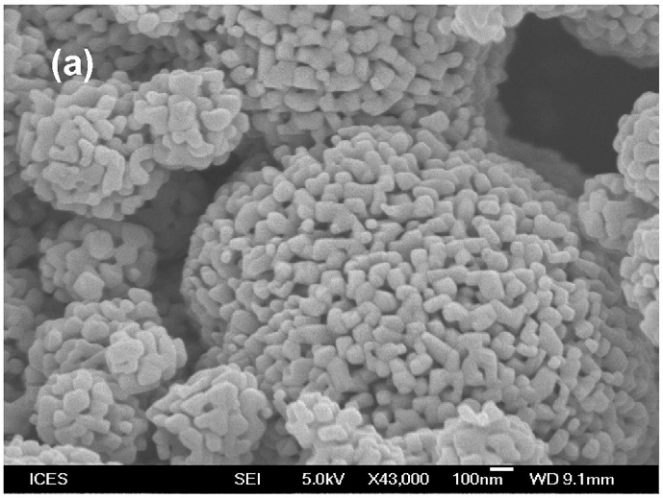

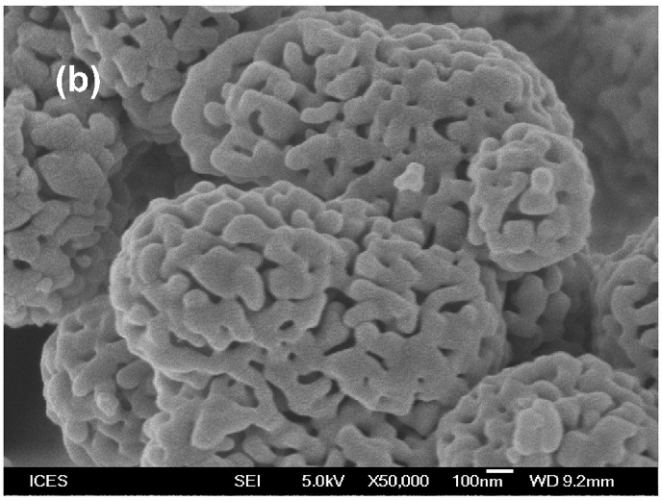

Fig. 4. SEM images of the α-Mn_2O_3 nanocrystals before (a) and after (b) reaction. The reaction was carried out in the stream of 0.5 kPa CH_4, 3.0 kPa O_2, in He, space velocity: 36,000 h^{-1}, at 550 °C for 10 h.

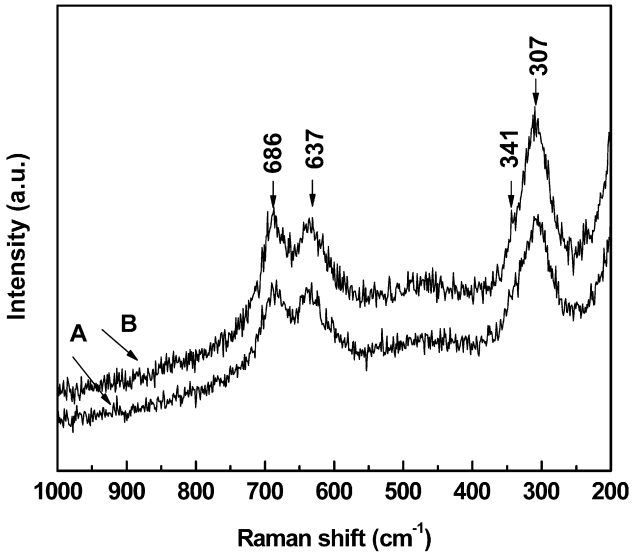

Fig. 5. Ex situ Raman spectra (normalized) of α-Mn_2O_3 nanocrystals as-prepared (A) and the spent catalyst (B). The reaction was carried out under the same conditions as in Fig. 3.

be extracted from those spectra even though the signals were remarkably attenuated (ca. 25% compared to ex situ spectra) because of the limitations of the technique. As shown in Fig. 6a, the spectrum obtained in He flow at 25 °C was similar to the ex situ spectra presented in Fig. 5. By increasing the temperature to 400 °C, the bands at 686 and 637 cm^{-1}, corresponding to the stretching vibrations of the bridged oxygen species, shifted to 678 and 622 cm^{-1}, respectively, accompanied with a decrease in their intensities. Moreover, a new band at 648 cm^{-1} with an onset at 400 °C and becoming intensive at 500 °C indicates the formation of a new phase. Surprisingly, the new band disappeared completely, and a spectrum corresponding to α-Mn_2O_3 was observed again when the temperature was returned to 25 °C in He flow, suggesting that this structural change is reversible. The temperature-dependent spectra obtained from CH_4 combustion, as shown in Fig. 6b, also showed a similar tendency, but the band at 648 cm^{-1} in He flow shifted up to 660 cm^{-1} at 450 °C with a weaker intensity; meanwhile, its intensity was reduced compared with that in He flow. It should be emphasized that this phenomenon was not clearly observed for the bulk α-Mn_2O_3 under the same experimental conditions.

In accordance with the previous Raman spectra obtained from various MnO_x samples [16,17,23,33], the band at 648 cm^{-1} formed at elevated temperatures, to be close to that (655 cm^{-1}) observed for the bulk Mn_3O_4 [16,17], is likely attributed to Mn–O–Mn stretching in Mn_3O_4. The general transition of MnO_x at elevated temperatures due to the loss of lattice oxygen has been described by [42]:

$$Mn_2O_3 \xrightarrow{900\,^\circ C} Mn_3O_4 \xrightarrow{1700\,^\circ C} MnO. \quad (3)$$

The formation of Mn_3O_4 from Mn_2O_3 occurs only when the calcination temperature is greater than 900 °C. However, the LRS spectra in Fig. 6a demonstrated that the transformation of α-Mn_2O_3 to Mn_3O_4-like species in He flow can even

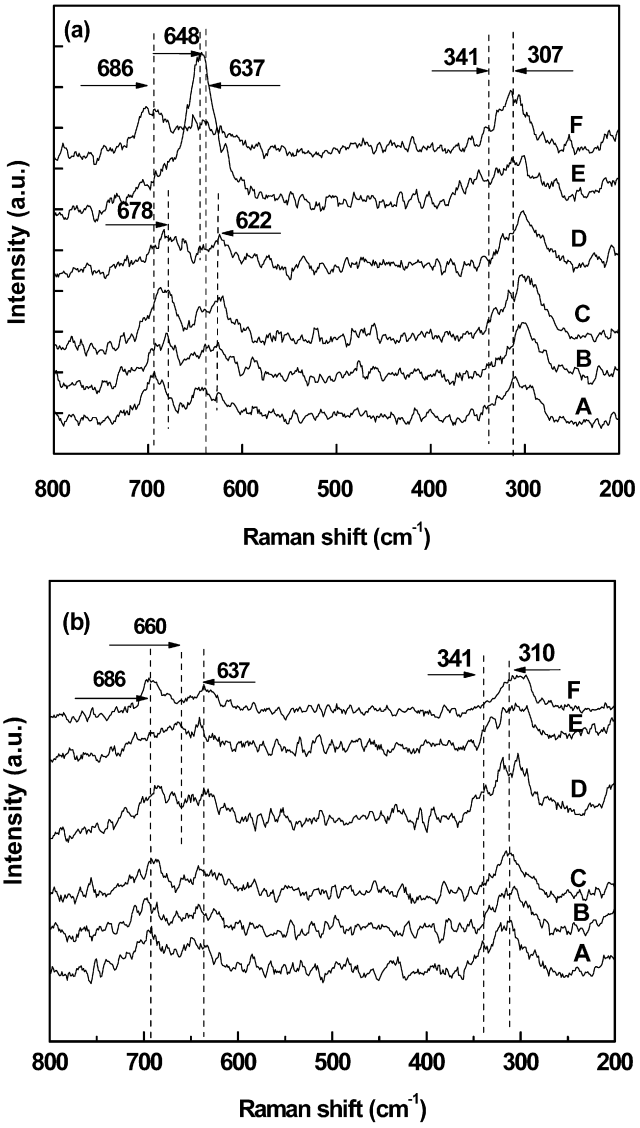

Fig. 6. Temperature-dependent in situ Raman spectra (normalized) for the α-Mn_2O_3 nanocrystals in the presence of He (a) and in the present of 0.5 kPa CH_4, 3.0 kPa O_2, in He (b); ramping rate: 10 °C/min; flow rate: 50 ml/min. (A) 25 °C, (B) 100 °C, (C) 200 °C, (D) 400 °C, (E) 500 °C, (F) back to 25 °C.

observed at temperatures as low as 400 °C, probably because of the loss of lattice oxygen that leads to a reconstruction of the phase. Interestingly, the feature for α-Mn_2O_3 vibrations reappeared after cooling to room temperature. However, the XRD spectra in Fig. 3 also demonstrate that there is almost no modification in the bulk structure after reaction. The reverse phase transformation might be caused by diffusion of oxygen from the bulk to the surface. Alternatively, supply of oxygen is possible from the gas phase during the reaction, as shown in Fig. 6b, that may suppress the phase-transformation. It may be a reason for the intensity of the band at 648 cm^{-1} in He flow to be stronger than the one at 660 cm^{-1} in methane combustion. In addition, the new band shift of 12 cm^{-1} in switching from He flow to CH_4 combustion may be caused by a change in local structure induced by the reactants. This phenomenon needs further study.

3.3. Plausible mechanism

The mechanism for the catalytic oxidation or combustion of hydrocarbons over metal oxide catalysts has long been debated [43]. Generally, those reactions are proposed to proceed through two pathways: (i) the Langmuir–Hinshelwood mechanism, where the reaction involves adsorbed reactants on the catalyst surface; (ii) and the Mars–van Krevelen mechanism, where the reactants are oxidized by lattice oxygen. In particular, the latter usually occurs at elevated temperatures, normally >500 °C. Several decades ago, Brooks also described that both mechanisms could be responsible for CO oxidation on MnO_x-based catalysts [44]. However, there is still no clear-cut understanding of this issue.

As for the present catalytic system, Figs. 1 and 2 reveal that below 450 °C the reaction orders and E_a over the nanocrystals are very close to those for the bulk, indicating that CH_4 is oxidized through the same mechanism for both catalysts. Below 450 °C in situ Raman spectroscopy (Fig. 6b) indicated that there were only minor structural modifications for the nanocrystal catalyst and no changes for the bulk (not shown for the sake of brevity). In combination with the positive reaction orders, we suggest that CH_4 combustion is mainly through a Langmuir–Hinshelwood mechanism. Likely, the surface CH_x reacts with adsorbed oxygen on the catalyst surface. Nevertheless, it still could not be precluded that a small amount of methane is oxidized simultaneously through the Mars–van Krevelen mechanism over both catalysts. The latter may become a predominant mechanism over the nanocrystal α-Mn_2O_3 above 450 °C, as indicated by the zero-order dependence on oxygen at 500 °C and the drastic drop in E_a, as listed Table 1. More interestingly, the change of the kinetic parameters occurs almost at the same temperature as for the formation of the Mn_3O_4-like species (Fig. 6).

It is well known that the catalytic activity of MnO_x at elevated temperatures depends strongly on the ability of manganese to be transferred into various oxidation states, e.g. Mn^{2+}/Mn^{3+} or Mn^{3+}/Mn^{4+}, and "oxygen mobility" in the oxide lattice. Therefore, the reversible phase-transformation between α-Mn_2O_3 and Mn_3O_4-like structures during reaction has important implications for the catalytic reaction. The lattice oxygen of MnO_x catalysts is considered to be the primary active species for activating the C–H bonds in hydrocarbons, as pointed out in a previous study [34], especially when the reaction temperature is above 400 °C, as illustrated by

$$CH_x\ (\text{ads}) + O^{2-}\ (\text{lattice}) + 2Mn^{4+/3+} \rightarrow CO_2\ (\text{ads}) + H_2O\ (\text{ads}) + 2Mn^{3+/2+}. \quad (4)$$

Our latest studies [34] have demonstrated that the activity of the α-Mn_2O_3 nanocrystals was considerably enhanced comparing with those of the bulk α-Mn_2O_3 and Mn_3O_4. Except for the relatively high surface area, the high mobility of lattice oxygen for the former should be a primary factor that leads to the enhancement of activity, because under similar conditions we did not observe any structural variations for the latter. Therefore, the zero-order dependence on oxygen at 500 °C and

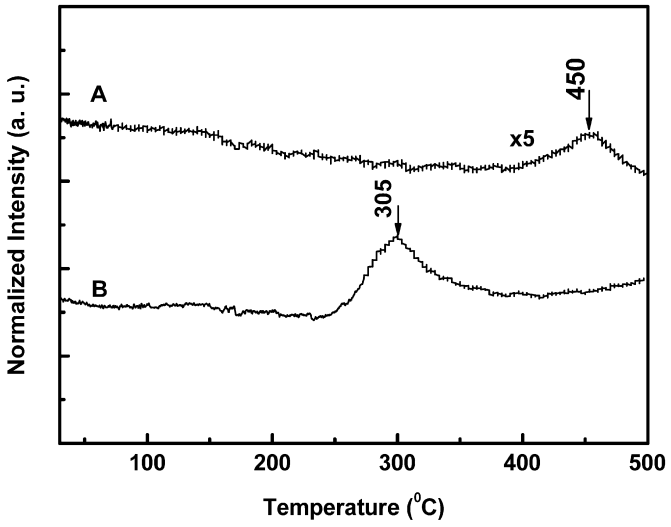

Fig. 7. O_2-TPD profiles for the "O_2-free" surface of bulk α-Mn_2O_3 (A) and α-Mn_2O_3 nanocrystal (B) with a N_2 flow rate of 50 ml/min, ramp rate of 20 °C/min, 50 mg of catalyst.

the reduction of the energy barrier observed for the α-Mn_2O_3 nanocrystals may be due to increased lattice oxygen participating in the reaction. This may also be the main reason for the superiority of the α-Mn_2O_3 nanocrystals to other MnO_x-based catalysts listed in Table 1. In order to demonstrate this mechanism, the mobility of lattice oxygen for both catalysts has been investigated through O_2 TPD experiments on so-called "O_2-free" and "O_2-precovered" surfaces. The spectra recorded from the "O_2-free" surface are shown in Fig. 7. The desorption of lattice oxygen appeared at 305 °C for the nanocrystals and 450 °C for the bulk; while the amount of desorbed oxygen was significantly reduced, about one tenth that measured for the bulk (12 μmol/g) compared to that for the nanocrystals (120 μmol/g). On the other hand, similar profiles were observed for the O_2-precovered surfaces, the amount of desorbed oxygen was 67 μmol/g for the former and 150 μmol/g for the latter, while the full monolayer of adsorbed oxygen was estimated to be about 423 μmol/g for the α-Mn_2O_3 nanocrystals and 106 μmol/g for the bulk. Likely, only part of surface was covered with adsorbed oxygen. In addition, the temperatures for the O_2 desorption over the nanocrystal α-Mn_2O_3 were lower than that for the onset of the phase modification identified by Raman spectroscopy. Perhaps, the formation of the new phase occurs only when a certain amount of surface oxygen is desorbed.

Clearly, through real-time in situ Raman spectroscopy we are able to observe a phase-transformation during CH_4 combustion over the α-Mn_2O_3 nanocrystals. The combination of kinetics and spectroscopy can explain the rise of high reactivity of the α-Mn_2O_3 nanocrystals. This study also helps gain insights into the mechanism of the oxidation of hydrocarbons over the MnO_x-based catalysts. Nevertheless, the role of the Mn_3O_4-like species formed during CH_4 combustion still needs further study.

4. Conclusions

Several conclusions can be drawn from this study. It is evident that the α-Mn_2O_3 nanocrystals prepared by oxidative decomposition of $MnCO_3$ have superior activity to bulk α-Mn_2O_3 in CH_4 combustion. At or below 450 °C, similar reaction orders and activation energy over both catalysts suggest that CH_4 is oxidized mainly through a Langmuir–Hinshelwood mechanism. With an increase in temperature the reaction over the nanocrystal α-Mn_2O_3 may gradually transfer to a Mars–van Krevelen mechanism, as indicated by the zero-order dependence on oxygen at 500 °C. On the contrary, the reaction mechanism over the bulk remains unchanged. Real-time in situ Raman spectroscopy has demonstrated that a reversible phase-transformation, forming a Mn_3O_4-like phase, might occur in the α-Mn_2O_3 nanocrystals during methane combustion. The phenomenon observed indicates that at elevated temperatures the lattice oxygen may be the primary active species that also leads to a reduction in the energy barrier to the reaction.

Acknowledgment

This study is supported by the Institute of Chemical Engineering and Sciences (ICES, A-STAR, Singapore) in-house project.

Supplementary material

The online version of this article contains additional supplementary material.

Please visit DOI: 10.1016/j.jcat.2007.11.010.

References

[1] A.J. Zarur, J.Y. Ying, Nature 65 (2000) 403.
[2] M.F.M. Zwinkels, S.G. Jaras, P.G. Menon, Catal. Rev. Sci. Eng. 35 (1993) 319.
[3] R.J. Charlson, Nature 438 (2005) 165.
[4] R.B. Anderson, K.C. Stein, J.J. Feenan, L.J.E. Hofer, Ind. Eng. Chem. 53 (1961) 809.
[5] J.R. Rostrup-Nielson, Catal. Rev. Sci. Technol. 46 (2004) 247.
[6] H.M. Zhang, Y. Teraoka, N. Yamazoe, Catal. Today 6 (1989) 155.
[7] D.L. Trim, Appl. Catal. 7 (1984) 249.
[8] J.J. Spivey, Ind. Eng. Chem. Res. 26 (1987) 2165.
[9] J.J. Spivey, J.B. Butt, Catal. Today 11 (1992) 465.
[10] J.R. Kittrell, J.W. Eldrige, W.C. Connor, Catalysis 9 (1991) 162.
[11] C. Kappenstein, T. Wahdan, D. Duprez, M.I. Zaki, D. Brands, E. Poels, A. Bliek, Stud. Surf. Sci. Catal. 91 (1995) 699.
[12] R. Radhakrishnan, S.T. Oyama, J. Catal. 199 (2001) 282.
[13] D. Döbber, D. Kießling, W. Schmitz, G. Wendt, Appl. Catal. B Environ. 52 (2004) 135.
[14] R. Kanaparthi, L.W. Chen, F. Chen, Z.Y. Zhong, J. Chin, H. Mook, Y.-F. Han, Catal. Commun. 8 (2007) 1421.
[15] B. Dmuchovsky, M.C. Freerks, F.B. Zienty, J. Catal. 4 (1965) 577.
[16] Y.-F. Han, F. Chen, Z.Y. Zhong, K. Ramesh, E. Widjaja, L.W. Chen, Catal. Commun. 7 (2006) 739.
[17] Y.-F. Han, F. Chen, Z.Y. Zhong, K. Ramesh, L.W. Chen, E. Widjaja, J. Phys. Chem. B 110 (2006) 24450.
[18] T. Yamashita, A. Vannice, Appl. Catal. B Environ. 13 (1997) 141.
[19] J.T. Kummer, Prog. Energy Combust. Sci. 6 (1979) 177.
[20] C.M. Julien, M. Massot, C. Poinsignon, Spectrochim. Acta Part A 60 (2004) 689.

[21] G. Le Bourdon, F. Adar, M. Moreau, S. Morel, J. Reffner, A.S. Mamede, C. Dujardin, E. Payen, Phys. Chem. Chem. Phys. 5 (2003) 4441.
[22] S.J. Tinnemans, J.G. Mesu, K. Kervinen, T. Visser, T.A. Nijhuis, A.M. Beale, D.E. Keller, AdM.J. van der Eerden, B.M. Weckhuysen, Catal. Today 113 (2006) 3.
[23] J. Zhang, M. Li, Z. Feng, J. Chen, C. Li, J. Phys. Chem. B 110 (2006) 927.
[24] M. Li, Z. Feng, Q. Xin, C. Li, Phys. Chem. Chem. Phys. 5 (2003) 5326.
[25] C. Li, M. Li, J. Raman Spectrosc. 33 (2002) 301.
[26] M.A. Banares, Catal. Today 100 (2005) 71.
[27] W. Li, G. Gibbs, S.T. Oyama, J. Am. Chem. Soc. 120 (1998) 9041.
[28] F. Kapteijn, A.D. van Langeveld, L.A. Moulijn, A. Andreini, J. Catal. 150 (1994) 94.
[29] F. Buciuman, F. Patcas, R. Cracium, D.R.T. Zahn, Phys. Chem. Chem. Phys. 1 (1999) 185.
[30] R. Radhakrishnan, S.T. Oyama, J. Phys. Chem. B 105 (2001) 9067.
[31] M. Ferrandon, J. Carnö, S. Järås, E. Björnbom, Appl. Catal. A Gen. 180 (1999) 141.
[32] B.R. Strohmeier, D.M. Hercules, J. Phys. Chem. 88 (1984) 4922.
[33] M.-C. Bernard, A.H.-L. Goff, B. Vu Thi, J. Electrochem. Soc. 140 (1993) 3065.
[34] Y.-F. Han, K. Ramesh, L.W. Chen, E. Widjaja, S. Chilukoti, F. Chen, J. Phys. Chem. C 111 (2007) 2830.
[35] C. Reed, Y. Xi, S.T. Oyama, J. Catal. 235 (2005) 378.
[36] P.B. Weisz, C.D. Prater, Adv. Catal. 6 (1954) 143.
[37] R.E. Hayes, S.T. Kolaczkowskib, P.K.C. Li, S. Awdry, Appl. Catal. B Environ. 25 (2000) 93.
[38] S. Cimino, L. Lisi, R. Pirone, G. Russo, M. Turco, Catal. Today 59 (2000) 19.
[39] H. Arai, T. Yamada, K. Eguchi, T. Seiyama, Appl. Catal. 26 (1986) 265.
[40] V. Pitchon, D.Yu. Murzin, Chem. Eng. Technol. 24 (2001) 12.
[41] R. Spinicci, A. Delmastro, S. Ronchetti, A. Tofanari, Mater. Chem. Phys. 78 (2002) 393.
[42] E.R. Stobbe, B.A. de Boer, J.W. Geus, Catal. Today 47 (1999) 161.
[43] L.D. Pfefferle, W.C. Pfefferle, Catal. Rev. 29 (1987) 219.
[44] C.S. Brooks, J. Catal. 8 (1967) 272.